Electrochemistry of Nanopore Electrodes in Low Ionic Strength Solutions

Yanhui Zhang, Bo Zhang, and Henry S. White*

Department of Chemistry, University of Utah, 315 South 1400 East, Salt Lake City, Utah 84112

Received: August 20, 2005; In Final Form: November 30, 2005

The steady-state voltammetric behavior of truncated conical nanopore electrodes (20−200 nm orifice radii) has been investigated in low ionic strength solutions. Voltammetric currents at the nanopore electrode reflect both diffusive and migrational fluxes of the redox molecule and, thus, are strongly dependent on the charge of the redox molecule and the relative concentrations of the supporting electrolyte and redox molecule. In acetonitrile solutions, the limiting current for the oxidation of the positively charged ferrocenylmethyltrimethylammonium ion is suppressed at low supporting electrolyte concentrations, while the limiting current for the oxidation of the neutral species ferrocene is unaffected by the ionic strength. The dependence of the limiting current on the relative concentrations of the supporting electrolyte and redox molecule is accurately predicted by theory previously developed for microdisk electrodes. Anomalous values of the voltammetric half-wave potential observed at very small nanopore electrodes (<50 nm radius orifice radii) are ascribed to a boundary potential between the pore interior and bulk solution (i.e., a Donnan-type potential).

Introduction

We report measurements of the influence of ion concentration on the electrochemical behavior of electrodes embedded at the bottom of deep nanopores. In a recent report, the fabrication of truncated, conical-shaped nanopore electrodes, schematically depicted in Figure 1, was described.[1] The nanopore electrode is prepared by sealing an atomically sharp Pt or Au wire in a glass capillary and polishing the capillary until a Pt or Au disk of nanometer dimensions is exposed. The exposed metal disk is then electrochemically etched to produce a truncated cone-shaped nanopore in glass, the bottom of the pore defined by a Pt disk electrode.

The nanopore electrode displays a well-defined sigmoidal-shape voltammetric response in the presence of a high concentration of an electrochemically inert electrolyte, corresponding to the diffusion-controlled transport of redox molecules through the pore orifice, followed by oxidation or reduction at the metal electrode. The diffusive flux of a redox molecule decreases rapidly as the pore depth increases and asymptotically approaches a constant value when the pore depth is ∼50 times larger than the pore orifice.[2] The asymptotic limit of the steady-state current is a consequence of the radial flux of molecules within the conical pore, is solely a function of the pore orifice radius and cone angle of the pore, and has a finite value for all cone angles greater than zero.[2]

Some potential applications of the nanopore electrode as an electrochemical sensor platform depend on the ability to make quantitative measurements in low ionic strength solutions, e.g., in environmental water analysis. Thus, in the present study, we have quantitatively examined the electrochemical behavior of nanopore electrodes as a function of the concentration of supporting electrolyte ions. The objectives of this work are to determine (1) whether the pore is sufficiently conductive, in low ionic strength solutions, to allow current flow without prohibitive ohmic losses and (2) whether electroneutrality within the pore interior can be maintained by ion transport through the pore orifice on the time scale of voltammetric measurements.

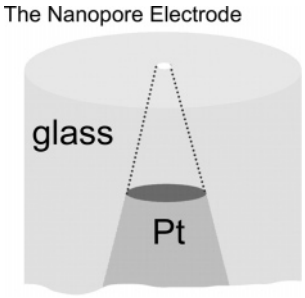

Figure 1. Schematic drawing of a glass nanopore electrode.

The issues of ion migration and electrical fields within the pore of a nanopore electrode are closely related to migrational transport at microdisk electrodes in low ionic strength media.[3−8] In solutions containing a very low concentration of supporting electrolyte, the flow of charge, i, results in an ohmic potential loss ($\Delta V = iR$) associated with a large solution resistance, R. In addition, the faradaic reaction generates a net electrical charge within the depletion layer which, in the absence of a sufficient quantity of supporting electrolyte, engenders migrational fluxes of both redox reactant and product. The influence of reaction-engendered fluxes was discussed in the early polargraphic literature[9] and later considered by Oldham,[6] Amatore,[5] and others[10] in developing a description of microelectrode voltammetry in low ionic strength solutions. Detailed mathematical descriptions of the voltammetric waveshape of microelectrodes as a function of the relative concentrations of supporting electrolyte and redox-active ion, $\gamma = C_{elec}/C_{redox}$, have been presented, with and without[11,12] assuming local electroneutrality and with the inclusion of homogeneous reactions.[13] In general, when $\gamma \gg 1$, the migrational fluxes of ions necessary to maintain charge balance with the depletion layer are negligibly small and the electrode reaction is diffusion controlled.

Figure 2 shows a comparison of computer-simulated concentration distributions of a redox-active molecule (e.g., ferrocene,

* To whom correspondence should be addressed. E-mail: white@chem.utah.edu.

10.1021/jp054704c CCC: $33.50
Published on Web 01/05/2006

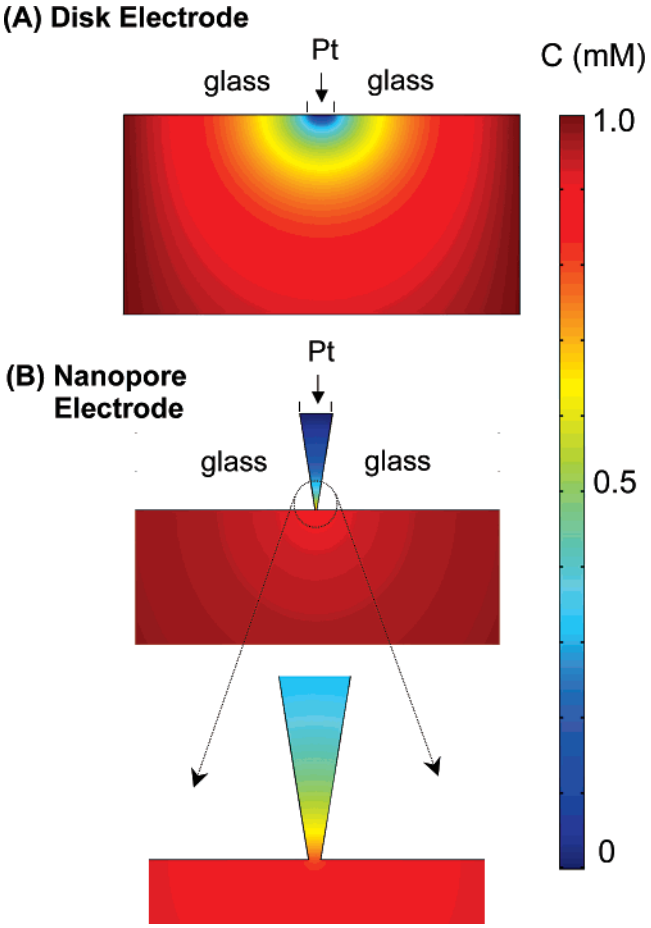

Figure 2. Finite-element simulations of the concentration distributions of a redox reactant at (A) a disk electrode and (B) a nanopore electrode (orifice radius = 50 nm and pore depth = 5 μm). In both (A) and (B), the diameter of the disk electrode is 1.86 μm and the bulk concentration of the reactant is 1 mM.

Fc), present at 1 mM in the bulk solution and undergoing a diffusion-limited reaction at the electrode surface, at (A) microdisk and (B) nanopore electrodes of equal electrochemically active areas (2.7 μm^2). In the nanopore electrode simulation, a pore orifice radius of 50 nm and a depth of 5 μm are assumed, values that are representative of experimentally achievable electrodes, as described below. The finite-element simulation results shown in Figure 2 were obtained using FEMLAB software, as detailed in a previous report[1] and are conceptually useful in identifying anticipated differences in the behaviors of the disk and nanopore electrodes in low ionic strength solutions. A key result of these simulations is that while the maximum concentration gradient at the microdisk electrode occurs at the electrode surface, it is displaced to the narrow end of the pore at the nanopore electrode, Figure 2B, a consequence of the conical shape of the pore.

Figure 3 shows a more quantitative comparison of (A) concentration profiles and (B) diffusional fluxes ($= -D\nabla C$) along the hypothetical centerline axes extending from the electrode surfaces into the bulk solution. Inspection of Figure 3B shows that the maximum flux at the nanopore electrode is ca. 3 times larger than that of the microdisk of equal electroactive area. In addition, Figure 3A demonstrates that essentially the entire depletion layer at the nanopore electrode occurs within the pore, extending only slightly into the bulk solution. Thus, in low ionic strength solutions, there are several unique constraints on ion transport at the nanopore electrode. First, the increased flux of redox molecules at the small opening of the

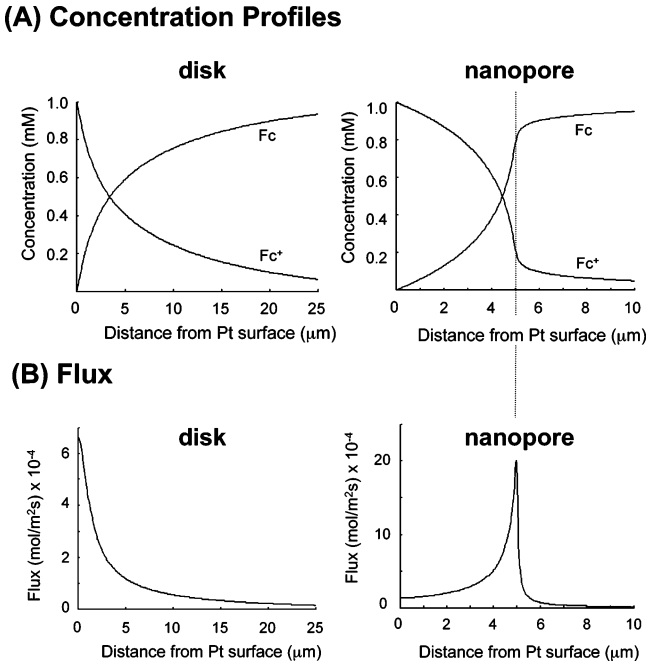

Figure 3. (A) Quantitative concentration profiles of reactant (Fc) and product (Fc^+), and (B) reactant flux, for the nanodisk and nanopore electrodes described in Figure 2. The orifice of the nanopore is located 5 μm from the Pt surface.

nanopore channel will result in the largest fraction of the ohmic potential loss occurring within this confined region, positioned micrometers away from the electrode surface. Second, because the reaction depletion layer is constrained to the pore interior (Figure 3), electroneutrality requires migration of electrolyte ions in and out of the pore during the voltammetric measurement. For sufficiently small pores, the pore resistance may be prohibitively large for quantitative voltammetric measurements. Additionally, specific chemical or physical interactions between the pore surface and ions may introduce novel transport behavior, such as current rectification reported in tapered quartz capillaries[14] and in membranes containing conical-shaped pores of nanometer radius.[15]

In the following sections, we describe the steady-state voltammetric response of nanopore electrodes with radii as small as 20 nm in acetonitrile solutions. We observe that nearly ideal voltammograms can be obtained at these electrodes for the oxidation of either neutral or positively charged redox molecules, even in the absence of any intentionally added supporting electrolyte. Although a small but measurable ohmic loss occurs within the pore channel, the voltammetric limiting currents are well described by existing theory for diffusional/migrational transport to microdisk electrodes. This latter result suggests that electroneutrality is maintained within the nanopores on the time scale of slow scan voltammetric experiments.

Experimental Section

Chemicals. Ferrocene (100%, Alfa Aesar), reagent grade H_2SO_4 (Fisher), $CaCl_2$, NaCN, NaOH, and acetone (Mallinckrodt Chemicals) were used without purification. HPLC grade acetonitrile (Sigma-Aldrich) was stored over 3-Å molecular sieves. Tetra-*n*-butylammonium hexafluorophosphate (Aldrich) was recrystallized from ethanol and dried under vacuum. Ferrocenylmethyltrimethylammonium hexafluorophosphate ($FcTMA^+PF_6^-$) was prepared by metathesis of ferrocenylmethyltrimethylammonium iodide (Alfa Aesar) with ammonium hexafluorophosphate (Aldrich) in water at ~60 °C for

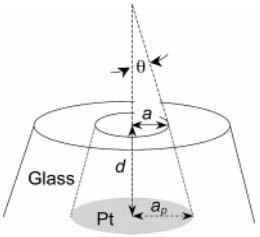

Figure 4. Schematic showing nanopore electrode geometrical parameters.

an hour, followed by recrystallization from water, and drying under vacuum.[16] Purified water (18 MΩ cm) was obtained from a Barnstead E-pure water purification system.

Electrochemical Apparatus. Steady-state voltammograms were obtained using a Cypress EI-400 bipotentiostat, interfaced to a computer through an AT-MIO16E-10 data acquisition board (National Instruments, NI) and controlled via a BNC-2090 analogue breakout accessory (NI). The high-sensitivity preamplifier (0.1−10 nA/V) of the bipotentiostat and a two-electrode cell positioned within a Faraday cage were used to measure $i-V$ curves at the nanometer-scale electrodes with minimal noise. The reference/auxiliary electrode was a commercial Ag/AgCl (3 M NaCl) electrode (Bioanalytical Systems) positioned ∼0.5 cm from the working electrode. Fast-scan voltammetry was preformed with a CHEM-CLAMP (Cornerstone Series) voltammeter-amperometer (Dagan Corporation) and a Princeton Applied Research Model 175 universal programmer (Princeton Applied Research). Transient waveforms were recorded with a LeCroy 9410 digital oscilloscope interfaced to a PC through a NI USB-to-GPIB controller, using in-house virtual instrumentation written in LABVIEW 6.0.

Nanopore Electrode. The preparation of nanopore electrodes has been described in detail in our previous reports.[1,2] Briefly, a Pt wire with a sharpened conical-shaped tip is sealed in a soda lime glass capillary, and the glass is polished to expose a Pt nanodisk electrode. The exposed Pt surface is then electrochemically etched in a $CaCl_2$ solution to create a conical pore in glass, with a Pt microdisk embedded at the bottom of the pore, as schematically depicted in Figure 4 (not drawn to scale). The key geometrical parameters that describe the pore geometry are orifice radius (a), electrode radius (a_p), pore depth (d), and half-cone angle (θ) (three of these four are independent parameters).

A procedure identical to that described in refs 1 and 2 was employed to make the electrodes reported here, with one modification to the methods used in sharpening Pt wires. In addition to etching Pt wire in basic 6 M NaCN/0.1 M NaOH solutions (method 1), we also employed a separate two-step procedure initially described by Libioulle et al.[17] and modified in our laboratory (method 2). A 25 μm diameter Pt wire was initially etched to a sharp point in an H_2O/acetone (v/v/2:1) solution containing 1.2 M $CaCl_2$ by applying 20 V alternating current (ac) between the Pt wire and a large-area Pt counter electrode. Bubbles were evolved at the Pt wire/solution interface during electrochemical etching; the applied voltage was removed immediately upon cessation of bubbling, and the Pt wire was washed with H_2O. The Pt tip was then resharpened in a 0.05 M H_2SO_4 solution by applying positive 15 V pulses (vs a large Pt electrode) of 16 μs duration at a repeating frequency of 4 kHz for 1 s. A −1.1 V direct current (dc) voltage was applied to the Pt wire for 10 s to reduce surface oxides. This process was repeated three times and completed by applying the −1.1 V dc voltage for 1 min. Method 2 yielded sharpened tips with significantly smaller half-cone angles (5 ± 1°) than method 1 (8 ± 1°).

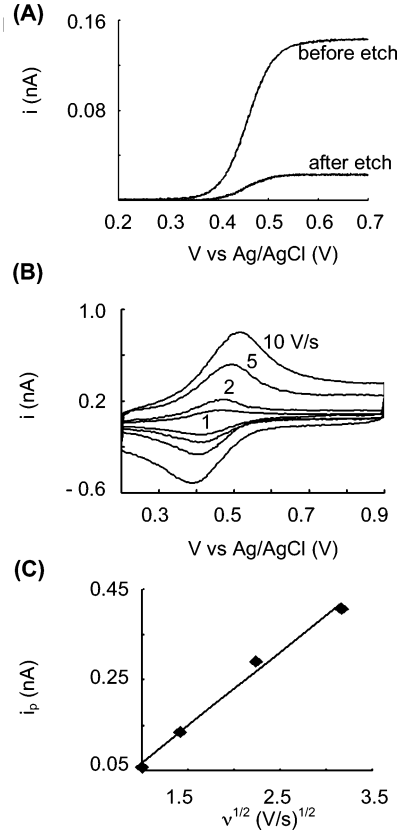

Figure 5. (A) Steady-state voltammetric response of a 150 nm radius orifice nanopore electrode in 20 mM $TBAPF_6/CH_3CN$ containing 1 mM Fc before (20 mV/s) and after (5 mV/s) the 20 s etch ($\theta = 8.1°$, $d = 12.8$ μm), (B) transient voltammetric response of the same electrode for $\nu = 1-10$ V/s, and (C) peak current plotted as a function of $\nu^{1/2}$.

Finite-Element Simulations. The concentration distributions presented in Figures 2 and 3 were obtained using Femlab v2.3 software (Comsol, Inc.) operated on a Dell Dimension XPS (Pentium 4 CPU, 3.2 GHz, 2 GB RAM). Details of the simulation procedure, the model geometry, and accuracy were previously given in ref 1.

Results and Discussion

Diffusion-Limited Response and Nanopore Electrode Geometry. Figure 5A shows the steady-state voltammetric response of a 150 (±5) nm radius Pt nanodisk electrode prepared from a sharpened wire with $\theta = 8°$ and the response of the corresponding Pt nanopore electrode (after etching the exposed Pt disk), both recorded in a 20 mM $TBAPF_6/CH_3CN$ solution containing 1 mM Fc. The radius of the nanodisk, a, is determined from the voltammetric limiting current[18]

$$i_{\lim}^{d=0} = 4nFDaC^* \tag{1}$$

where n is the number of electrons transferred per molecule, F is the Faraday constant, and D (2.4×10^{-5} cm^2/s)[19] and C^* are the diffusion coefficient and bulk concentration of the redox molecule, respectively. The diffusion-limited steady-state current at a nanopore electrode is given by eq 2

$$i_{\lim} = 4nFaDC^* \left[\frac{1 + (d/a)\tan\theta}{4d/a\pi + (1 + (d/a)\tan\theta)}\right] \tag{2}$$

which is valid to within 5% for $\theta < 20°$.[2] When the pore depth

d is much larger than the orifice radius a ($d/a > 50$), the limiting current asymptotically approaches a value which depends only on θ and a, eq 3.

$$i_{\lim}^{d\to\infty} = 4nFaDC^* \left[\frac{\tan\theta}{4/\pi + \tan\theta}\right] \quad (3)$$

Application of eqs 2 and 3 to the analysis of voltammetric data requires measurements of a, d, and θ. The value of a in eqs 2 and 3 is also equal to the radius of the Pt disk prior to etching the Pt, eq 1, assuming that the geometry of the pore walls, after etching, faithfully reproduces the shape of the original Pt wire surface. Using scanning electron microscopy, we have previously demonstrated that the orifice radius is within 20% of the original Pt disk radius after etching the Pt in the $CaCl_2$ solution and that both pore orifice and Pt disk have disk geometries. Optical microscopy is used to measure θ to within 1°.

The remaining geometrical parameter d is determined by measuring the radius, a_p, of the Pt disk embedded within the pore, and using geometrical relationships along with the values of a and θ to compute d. To determine d, we note that the current becomes limited by planar diffusion of redox molecules initially present in the pore at sufficiently high voltammetric scan rates. In this limit, the voltammetric response of the nanopore electrode is identical to that of a macroscopic planar electrode.[20] The value of a_p is determined from the slope of a plot of the voltammetric peak current, i_p, vs the square root of the scan rate, $\nu^{1/2}$, using the expression for i_p at a shielded planar electrode under diffusion current, eq 4.

$$i_p = 2.69 \times 10^5 n^{3/2} D^{1/2} C^* \nu^{1/2} \pi a_p^{\,2} \quad (4)$$

Figure 5B shows the voltammetric response of the 150 nm radius pore electrode at scan rates from 1 to 10 V/s, and Figure 5C shows the corresponding linear plot of i_p vs $\nu^{1/2}$. The slope of this plot corresponds to $a_p = 2.0$ μm, from which a pore depth, d, of 12.8 μm is computed. Since $d/a \sim 85 > 50$, eq 3 can be used to estimate the anticipated limiting current at the nanopore electrode. Employing the measured value of $\theta = 8°$ yields $i_{\lim}^{d\to\infty} = 0.1 i_{\lim}$. In other words, etching the pore to an arbitrary depth greater than $\sim 50a$ results in a current that is anticipated to be ~10% of the limiting current prior to etching. We observe a value of $i_{\lim}^{d\to\infty}$ that is slightly higher than this predicted value (Figure 5A). However, the agreement is sufficient for the investigations described below, which are based on the relative magnitudes of voltammetric currents at different electrolyte concentrations and, thus, do not require precise knowledge of the pore geometry. The geometry of other nanopore electrodes were determined by the same procedure.

Voltammetry in Low Ionic Strength Solutions. The oxidations of a neutral (ferrocene, Fc) and a charged (ferrocenylmethyltrimethylammonium cation, $FcTMA^+$) redox molecule were investigated at nanopore electrodes in CH_3CN solutions containing various amounts of $TBAPF_6$ as the supporting electrolyte. The response of the corresponding Pt nanodisk prior to generating the pore was also recorded in order to quantify the influence of the pore on the voltammetric response.

Figure 6A shows the voltammetric response of an 86 nm radius nanodisk electrode in 2 mM $FcTMA^+$ solution at 20 mV/s for [$TBAPF_6$] corresponding to $\gamma = C_{elect}/C_{redox} = 0$, 1, 5, and 20. Inspection of Figure 6A shows that the limiting current decreases as γ decreases. The dependency of current on the supporting electrolyte concentration results from the electrochemical generation of the dication $FcTMA^{2+}$ at the electrode surface which, in the absence of excess supporting electrolyte, electrostatically repels $FcTMA^+$, thereby reducing the flux of reactant to the electrode surface (and thus the current). Qualitatively, a similar behavior has been reported by other researchers and by us using disk electrodes of micrometer dimensions.[10,21−23]

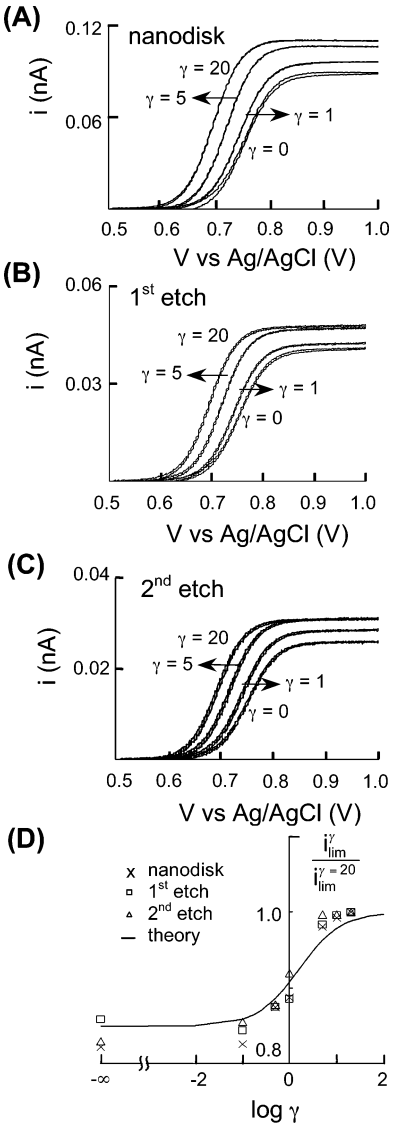

Figure 6. Steady-state voltammetric response of an 86 nm radius nanopore electrode in 2 mM $FcTMAPF_6/CH_3CN$ containing $TBAPF_6$ for $\gamma = 0-20$: (A) nanodisk electrode before etch (20 mV/s), (B) after 1st 5 s etch (10 mV/s), (C) after a 2nd 20 s etch (2 mV/s), and (D) plot of $i_{\lim}^{\gamma}/i_{\lim}^{\gamma=20}$ vs log γ for nanodisk and nanopore electrodes and comparison to theory, eq 5.

Amatore et al. have reported an expression for the ratio of the limiting current at arbitrary γ ($i_{\lim}^{\gamma}$) relative to the value in the presence of an excess concentration of electrolyte, $\gamma \gg 1$ ($i_{\lim}^{\gamma\to\infty}$), eq 5. For the steady-state one-electron (1-e) oxidation of a singly charged cation ($z = 1$)[24]

$$\frac{i_{\lim}^{\gamma}}{i_{\lim}^{\gamma\to\infty}} = 1 - [(3+4\gamma)^2 - 12\gamma(1+\gamma)]^{1/2} + [(4+4\gamma)^2 - 12\gamma(1+\gamma)]^{1/2} + 4(1+\gamma) \times \ln\frac{3+4\gamma+[(3+4\gamma)^2 - 12\gamma(1+\gamma)]^{1/2}}{4+4\gamma+[(4+4\gamma)^2 - 12\gamma(1+\gamma)]^{1/2}} \quad (5)$$

In the absence of any added supported electrolyte, eq 5 predicts that the voltammetric current is reduced to ~85% of the diffusion-limited value, in good agreement with results for the nanodisk electrode; see Figure 6.

After etching the Pt in a 15% $CaCl_2$ solution to generate a nanopore electrode ($\theta \sim 7°$), the above set of measurements was repeated to determine the dependence of limiting currents on electrolyte concentration. Figure 6B shows the set of voltammograms at $\gamma = 0$, 1, 5, and 20 after etching the Pt for 5 s to generate a very shallow pore.[25] Figure 6C shows a third set of voltammograms after re-etching the nanopore electrode for an additional 20 s to generate a significantly deeper pore (4.6 μm). Inspection of parts A−C of Figure 6 suggests that the dependence of the voltammetric current on γ is independent of pore depth and that the nanopore electrode behavior similarly to the microdisk. Figure 6D shows a quantitative comparison of the data with eq 5, which gives a remarkably good prediction of the dependence of $i_{lim}^{\gamma}/i_{lim}^{\gamma\to\infty}$ over ca. 4 orders of magnitude variation in γ. In plotting the data in Figure 6D, we have normalized the measured current at arbitrary γ to the value measured at $\gamma = 20$. The latter value corresponds to a sufficient excess of supporting electrolyte to ensure an essentially diffusion-controlled response. The point labeled $\log \gamma = -\infty$ in Figure 6D corresponds to solutions in which no supporting electrolyte was intentionally added. Of course, impurity ions act as the supporting electrolyte; we previously estimated a typical minimum impurity ion concentration of several tens of nM in CH_3CN solutions.[26] Thus, the value $\log \gamma = -\infty$ corresponds to the more physically realistic range of $-5 < \log \gamma < -3$.

The oxidation of 1 mM Fc in CH_3CN containing $TBAPF_6$ at concentrations ranging from 0 to 50 mM was also investigated at nanodisk and nanopore electrodes. While the oxidation of Fc generates a cation (Fc^+) at the electrode surface (and within the nanopore), no dependence of $i_{lim}^{\gamma}/i_{lim}^{\gamma\to\infty}$ on γ is anticipated because the flux of the reactant Fc is purely diffusional for all solution conditions. This prediction is borne out in the voltammetric data at nanodisk and nanopores of different pore depths. For example, Figure 7 shows the voltammetric response for Fc oxidation at 70 nm radius nanodisk electrode, and the response following electrochemically etching of the Pt in a $CaCl_2$ solution to create shallow (1st etch) and deep (2nd etch, $d = 6.5$ μm) pores. The voltammetric current in these experiments decreases by a few percent as γ increases due to a small increase in CH_3CN solution viscosity at $TBAPF_6$ concentrations above 10 mM.[27]

Figure 8 shows a summary plot of $i_{lim}^{\gamma}/i_{lim}^{\gamma=20}$ vs $\log \gamma$ for nanodisk and nanopore electrodes for the (A) oxidation of $FcTMA^+$ (9 nanodisk and 13 nanopore electrodes) and the (B) oxidation of Fc (8 nanodisk and 12 nanopore electrodes), the associated error, and a comparison to the theoretical prediction of eq 5. It is clear the voltammetric current at the nanopore electrode is well described by diffusion/migration theory developed for the microdisk electrode. Since eq 5 is based on the assumption that local electroneutrality is maintained everywhere (except within the double layer), this finding suggests that electroneutrality is maintained within the pore during the voltammetric measurement.

Half-Wave Potentials and Ohmic Potential Drop in the Nanopore. The voltammetric half-wave potential, $E_{1/2}$, at microelectrodes is also sensitive to γ, reflecting the increase in solution resistance as the supporting electrolyte concentration is decreased. For instance, in Figure 6, a positive 54 mV shift is observed at the 86 nm radius nanodisk electrode for the

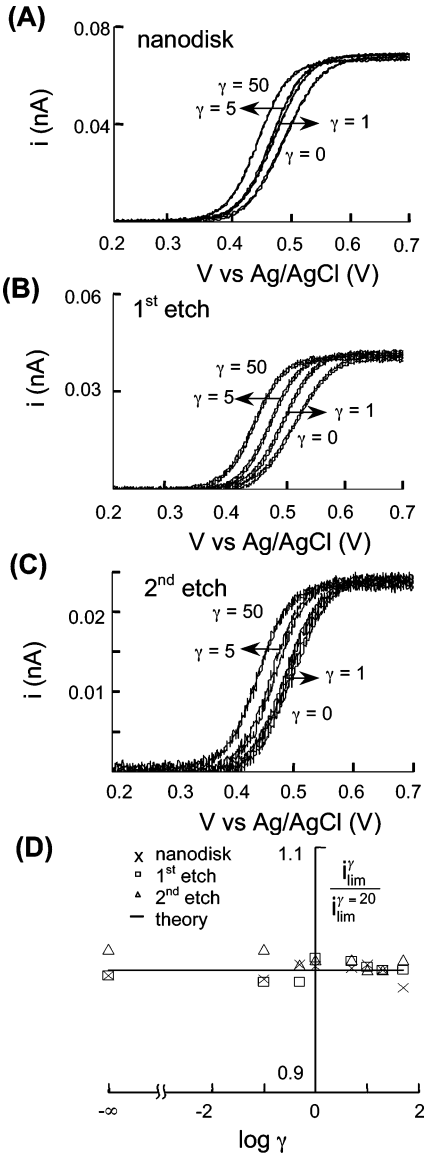

Figure 7. Steady-state voltammetric response of a 70 nm radius nanopore electrode in 1 mM Fc/CH_3CN containing $TBAPF_6$ for $\gamma = 0-50$: (A) nanodisk electrode before etch (20 mV/s), (B) after 1st 5 s etch (5 mV/s), (C) after 2nd 20 s etch (5 mV/s) ($d = 6.5$ μm, $\theta = 10°$), and (D) plot of $i_{lim}^{\gamma}/i_{lim}^{\gamma=20}$ vs $\log \gamma$ for nanodisk and nanopore electrodes and comparison to theory, eq 5.

oxidation of $FcTMA^+$ when γ is reduced from 20 to 0. Surprisingly, we find that the dependence of $E_{1/2}$ on γ at the nanopore electrodes is essentially the same as it is at the corresponding nanodisk, suggesting that transport of electrical charge through pore, even in the absence of any supporting electrolyte, does not introduce a significant additional ohmic potential loss. $FcTMA^+$ oxidation in the pore generates $FcTMA^{2+}$, leading to a transient redistribution of PF_6^- counterions in order to maintain local charge neutrality. This transport of PF_6^- counterions tends to counter the build-up of local electric fields, which contributes to the lack of a significant ohmic drop within the pore.

The oxidation of the neutral Fc at the nanopore electrode is a more stringent measure of the ohmic loss within the pore, as this redox molecule does not carry a counterion with it into the solution. Thus, in low ionic strength solutions, there are few counterions to prevent the build-up of electric fields. We consistently observe that the shift in $E_{1/2}$ for Fc oxidation is significantly larger at the nanopore electrode than at the nanodisk

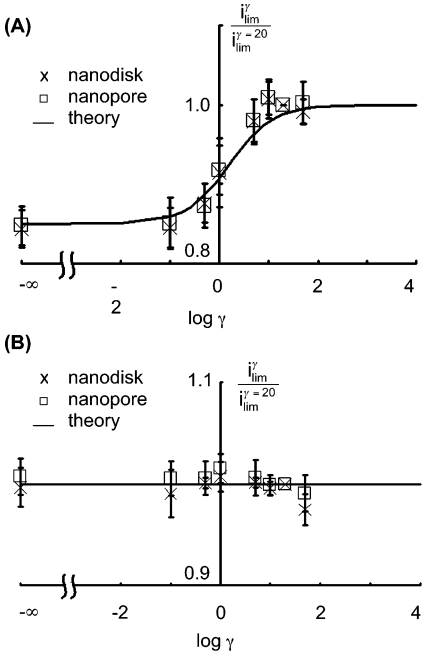

Figure 8. Plot of $i_{lim}^{\gamma}/i_{lim}^{\gamma=20}$ vs log γ for nanodisk and nanopore electrodes and comparison to theory (eq 5) for the (A) oxidation of $FcTMA^+$ (nanodisk, $n = 9$, and nanopore, $n = 13$, n is the number of trials; electrode radius: $30 \le a \le 328$ nm) and (B) oxidation of Fc (nanodisk, $n = 8$, and nanopore, $n = 12$; electrode radius: $20 \le a \le 115$ nm).

TABLE 1: $E_{1/2}$ for Fc Oxidation at 92 nm radius Pt Nanodisk and Nanopore Electrodes[a]

γ	nanodisk[b]	nanopore[b] (1st etch)	nanopore[b] (2nd etch)
0	0.48_3 V[c]	0.52_1	0.53_2
0.1	0.47_8	0.51_7	0.52_2
0.5	0.48_8	0.51_1	0.50_8
1	0.48_6	0.50_3	0.50_7
10	0.46_4	0.46_4	0.46_8
20	0.45_9	0.45_9	0.45_9

[a] Values in $CH_3CN/TBAPF_6$ solutions containing 1 mM Fc. [b] Same electrode, prior to and following the etch. [c] vs Ag/AgCl (3 M NaCl).

electrode. For instance, Table 1 lists $E_{1/2}$ values for a 92 nm radius nanodisk electrode and the corresponding nanopore electrodes after a first and second etch to produce shallow and deep pores, respectively. $E_{1/2}$ values for the nanopore electrodes tend to be several tens of millivolts more positive than at the nanodisk electrode when $\gamma < 1$, a difference that disappears when an excess of supporting electrolyte is present in solution. Although the difference in $E_{1/2}$ is small, it suggests that the pore is quite resistive. The limiting current for a 92 nm radius nanopore electrode is ~0.1 nA. To generate a 30 mV ohmic loss, relative to the "nonpore" ohmic loss at the corresponding nanodisk electrode, requires a pore resistance in the range 0.1 to 1 GΩ during the voltammetric scan. This resistance reflects the ion contributions from the redox reaction and the ion distribution from the surface counterions and impurity ions (e.g., from leakage of the Ag/AgCl (3 M NaCl) reference electrode). A more complete analysis of the pore resistance is currently being undertaken and will be reported at a later date.

Finally, we note interesting preliminary observations of anomalous shifts in $E_{1/2}$ for Fc oxidation at the three smallest nanopore electrodes ($a < 50$ nm) employed in this study. For instance, at one 48 nm radius nanopore electrode, we found $E_{1/2}$ to be essentially independent of γ, even though the normal positive shift in $E_{1/2}$ with decreasing γ was observed at the

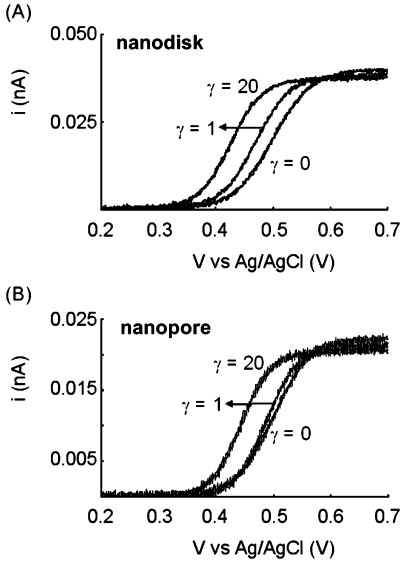

Figure 9. Steady-state voltammetric response of a 21 nm radius (A) nanodisk (20 mV/s) and (B) nanopore electrode (5 mV/s) in 2 mM Fc/CH_3CN containing $TBAPF_6$ for $\gamma = 0$, 1, and 20.

corresponding nanodisk electrode. A more representative example is shown in Figure 9, where a much smaller shift in $E_{1/2}$ at low γ is observed at a 21 nm radius nanopore electrode than at the corresponding nanodisk electrode. The reproducibility of this behavior is not great between different electrodes, indicating lack of control over the pore geometry at this length scale. However, the decrease in dependence of $E_{1/2}$ at the smallest nanopore electrodes suggests that the ion concentration in the pore is regulated by local surface chemistry, rather than simply reflecting the bulk ion concentration. This is essentially equivalent to a Donnan potential between the pore interior and the bulk solution[20] and, with further development, may have utility in making potentiometric measurements on nanometer length scales.

Conclusions

Our investigations demonstrate that it is possible to make quantitative voltammetric measurements using nanopore electrodes in low ionic strength solutions. Even in the absence of any intentionally added supporting electrolyte or redox ions (as in the case of Fc oxidation), the ohmic potential loss within the pore is small and does not dominate the electrode response. The faradaic currents generated at these electrodes reflect both migration and diffusion of redox species through the pore orifice and are accurately described, for oxidation of both charged and neutral molecules, using transport theory based on the assumptions of Nernst−Planck transport and electroneutrality. Because eq 5 is not a function of the chemical nature of the solvent, we anticipated that this conclusion will generally extend to other redox molecule/solvent systems.

Acknowledgment. This research was supported by the National Institutes of Health and by an American Chemical Society, Division of Analytical Chemistry Fellowship to B.Z., sponsored by the Society of Analytical Chemists of Pittsburgh. The authors thank Prof. M. Meyerhoff for pointing out the possibility of observing Donnan potentials in nanopore electrodes.

References and Notes

(1) Zhang, B.; Zhang, Y.; White, H. S. *Anal. Chem.* **2004**, *76*, 6229.
(2) Zhang, B.; Zhang, Y.; White, H. S. *Anal. Chem.* **2005**, in press.

(3) Howell, J. O.; Wightman, R. M. *Anal. Chem.* **1984**, *56*, 524.
(4) Amatore, C.; Deakin, M. R.; Wightman, R. M. *J. Electroanal. Chem.* **1987**, *220*, 49.
(5) Amatore, C.; Fosset; B.; Bartelt, J.; Deakin, M. R.; Wightman, M. R. *J. Electroanal. Chem.* **1988**, *256*, 255.
(6) Oldham, K. B. *J. Electroanal. Chem*. **1988**, *250*, 1.
(7) Oldham, K. B. *J. Electroanal. Chem.* **1992**, *337*, 91.
(8) Myland, J. C.; Oldman, K. B. *J. Electroanal. Chem.* **1993**, *347*, 49.
(9) Kolthoff, I. M.; Ligane, J. J. *Chem. Rev.* **1939**, *24*, 1.
(10) An excellent overview of experimental studies and the theoretical development of voltammetry in low ionic strength solutions is found in Zoski, C. G. In *Modern Techniques in Electroanalysis*; Vanysek, P., Ed.; Wiley: New York, 1996; pp 241−312.
(11) (a) Smith, C. P.; White, H. S. *Anal. Chem*. **1993**, *65*, 3343. (b) Norton, J. D.; White, H. S.; Feldberg, S. W. *J. Phys. Chem.* **1990**, *94*, 6772.
(12) Oldham, K. B.; Bond, A. M. *J. Electroanal. Chem*. **2001**, *508*, 28.
(13) (a) Norton, J. D.; Benson, W. E.; White, H. S.; Pendley, B.; Abruña, H. D. *Anal. Chem*. **1991**, *63*, 1909. (b) Amatore, C.; Paulson, S. C.; White, H. S. *J. Electroanal. Chem.* **1997**, *439*, 173.
(14) Wei, C.; Bard, A. J.; Feldberg, S. W. *Anal. Chem.* **1997**, *69*, 4627.
(15) (a) Siwy, Z.; Dobrev, D.; Neumann, R.; Trautmann, C.; Voss, K. *Appl. Phys. A* **2003**, *76*, 781. (b) Siwy, Z.; Heins, E.; Harrell, C. C.; Kohli, P.; Martin, C. R. *J. Am. Chem. Soc.* **2004**, *126*, 10850.
(16) White, H. S.; Leddy, J.; Bard, A. J. *J. Am. Chem. Soc.* **1982**, *104*, 4811.
(17) Libioulle, L. Houbion, Y. Gilles, J.-M. *Rev. Sci. Instrum.* **1995**, *66*, 97.
(18) Saito, Y. *Rev. Polarogr*. **1968**, *15*, 177.
(19) Bond, A. M.; Henderson, T. L. E.; Mann, D. R.; Thormann, W.; Zoski, C. G. *Anal. Chem.* **1988**, *60*, 1879.
(20) Bard, A. J.; Faulkner, L. R. *Electrochemical Methods*, 2nd ed.; John Wiley & Sons: New York, 2001.
(21) Lee, C.; Anson, F. C. *J. Electroanal. Chem*. **1992**, *323*, 381.
(22) (a) Cooper, J. B.; Bond, A. M. *Anal. Chem.* **1993**, *65*, 2724. (b) Bond, A. M.; Pfund, V. B. *J. Electroanal. Chem.* **1992**, *335*, 281.
(23) (a) Ciszkowska, M.; Stojek, Z. *J. Electroanal. Chem.* **1993**, *344*, 135. (b) Stojek, Z.; Ciszkowska, M.; Ostereyoung, J. G. *Anal. Chem*. **1994**, *66*, 1507. (c) Ciszkowska, M.; Osteryoung, J. G. *J. Phys. Chem*. **1994**, *98*, 3194.
(24) Equation 3 is obtained from eq 30 of ref 5, using $z = +1$ and $n = -1$.
(25) The pore is too shallow to observe a peak-shape planar diffusion response, even at $\nu = 50$ V/s. Thus, the depth of this pore is undetermined.
(26) Pendley, D. B.; Abruna, H. D.; Norton, J. D.; Benson, W. E.; White, H. S. *Anal. Chem*. **1991**, *63*, 2766.
(27) Gao, X.; White, H. S. *Anal. Chem.* **1995**, *67*, 4057.